Arch Appl Mech (2012) 82:515–531
DOI 10.1007/s00419-011-0570-8

ORIGINAL

E. Kreuzer · M. Steidl

Controlling torsional vibrations of drill strings via decomposition of traveling waves

Received: 9 May 2011 / Accepted: 7 July 2011 / Published online: 26 July 2011

Abstract Torsional vibrations in drill strings, especially stick-slip vibrations, are detrimental to the drilling process as they slow down the rate of penetration and may lead to failure of the drilling equipment. We present a method for controlling these vibrations by exactly decomposing the drill string dynamics into two traveling waves traveling in the direction of the top drive and in the direction of the drill bit. The decomposition is derived from the wave equation governing the string vibrations and is achieved with only two sensors that can be placed directly at the top drive and at a short distance below the top drive (e.g., 5 m). Therefore, downhole measurements along the string and at the bit are not necessary, which is a major advantage compared to other control concepts for drill string dynamics. The velocity of the top drive is then controlled in order to absorb the wave traveling in the direction of the top drive, thus achieving a reflection coefficient of zero for the frequency range of the undesired torsional vibrations. The proposed algorithm is implemented for both a numerical example and an experimental setup; results show that the control concept works very effectively.

Keywords Stick-slip vibrations · Drill string · Decomposition of traveling waves · Control

1 Introduction

Drill strings used to drill for oil and gas have a typical length of several kilometers. Due to its extensive length, the diameter-to-length ratio of a drill string is extremely small (smaller than that of a human hair). At the lower end of the string, the drill bit is subjected to friction occurring between drill bit and rock. The friction characteristic depends on the rock formation, but often is of strongly nonlinear character. A falling friction coefficient over angular velocity of the friction characteristic may lead to instability of the angular motion and the onset of self-excited stick-slip vibrations with large amplitudes. Here, the drill bit comes to a complete standstill, while, due to constant velocity at the top drive, the string winds up. Once the torque at the bit exceeds the sticking friction, the string unwinds rapidly beyond its equilibrium position and the bit comes to another standstill. As friction characteristics may change during the drilling process and as the string may be subjected to various unknown and time-variant external forces and disturbances not only at the bit, but also along the string, several different operational regimes may occur while drilling. Therefore, the amplitude and frequency of the stick-slip vibrations may vary from regular to very irregular vibrations, depending on the friction characteristic between bit and rock or the occurrence of additional friction or disturbances along the string.

E. Kreuzer (✉) · M. Steidl
Institute of Mechanics and Ocean Engineering, Hamburg University of Technology,
Eissendorferstr. 42, Hamburg 21073, Germany
E-mail: kreuzer@tuhh.de
Tel.: +49-40-42878 3220
Fax: +49-40-42878 20 28

As drilling is very expensive and as undesired, stick-slip vibrations are detrimental to the drilling process due to lower rate of penetration and even damage of the drill string (compare e.g., [1]); the problem and possible remedies have attracted a lot of interest from the scientific community. Early approaches aimed at optimizing the drill string configuration in a way that stick-slip vibrations are less likely to occur, [4] or [15], for example via variation in weight on bit or angular velocity of the string. Other approaches develop controllers using classical concepts from control theory like robust μ-synthesis ([7]) or $\mathcal{H}_\infty$-control ([14]). These approaches require a good model of the drill string, and the external loads acting upon it. A different approach is taken in [8,10] and [17]; here, the relevant dynamics of the drill string are analyzed with Karhunen–Loève-Transform or Proper Orthogonal Decomposition, which requires measurements along the string. Although new technology is available, which allows measurements along the string while drilling, it is very expensive to obtain these measurements, while for conventional drilling setups, virtually no information about the dynamics along the string is available, as no measurements are taken along the string. Measurements are recorded at the bit, but standard measurement-while-drilling devices send this information to the top via mud-pulse technology that uses the liquid between the string and the borehole to transmit pulses. The bit rate here is only between ten and 40 bps, and, more relevant, the time the pulses take to travel to the top is longer than the traveling time of torsional waves, as the velocity of torsional waves in drill strings is normally $c = \sqrt{G/\rho}$ with shear modulus G and density ρ, which is approximately 3,000 m/s for typical steel drill strings, while the propagation speed of the pulses is about 1,700 m/s (speed of sound in oil). Other control algorithms focus on the fact that the torsional vibrations are governed by the wave equation, and each torsional vibration is a superposition of a wave traveling up the string and a wave traveling down the string. In order to eliminate vibration energy from the string, the reflection coefficient of the top drive should be small for the relevant stick-slip frequencies. In [5,6,18], control concepts are presented, which achieve a low reflection coefficient for a certain frequency band.

Often, torsional vibrations occur as a result of nonlinear effects like stick slip of the bit or the string sticking to the borehole wall and breaking loose due to differential sticking. As a consequence of these nonlinearities, the vibrations may contain a wide variety of frequencies and an optimal control would require knowledge of the evolution over time of the wave traveling in direction of the actuator, thus being able to completely compensate the traveling wave in the top drive and keeping the reflection coefficient zero for the complete relevant frequency range. In this paper, we present an exact decomposition of traveling waves in a continuum governed by the wave equation. We achieve the decomposition by exploiting the finite traveling speed of waves in the continuum and the corresponding delay between two measurement points. The two measurement points can be located close to the top drive; hence, downhole measurements are not necessary, a major advantage compared to other control concepts for drill strings. By adding the decomposed wave traveling in the direction of the top drive to the top drive velocity, the top drive acts as boundary controller that compensates the wave traveling in the direction of the boundary. A reflection of undesired torsional vibrations back into the drill string is prevented, thus absorbing the maximum amount of energy. The control concept therefore works in the way that it virtually removes the boundary of the drill string, and the dynamics behave as if the string was infinitely stretched out instead of being bounded by the top drive.

Results from numerical simulations and from an experimental setup show that the stick-slip vibrations can be suppressed very effectively with the proposed method. At the same time, no measurements along the string are necessary and it is sufficient to measure the rotational speed of the string between the top and a couple of meters below the top to stabilize the whole string.

The paper is organized as follows: we first present the model of the drill string used for numerical simulations and the resulting stick-slip dynamics for two different friction scenarios. We then derive the control concept that is based on the decomposition of traveling waves via sensor measurements close to the top drive. In the following chapter, we apply the control concept to the model and show results. Finally, we present a short overview of our experimental setup and show results from the application of the control concept on our experimental setup.

2 Drill string model

A typical drill string configuration is shown in Fig. 1. It consists of three main components:

– **Top Drive**
  The top drive very often is a high-torque AC Motor that is hoisted in the drilling rig and turns the string. The mass moment of inertia of the top drive motor is given by J_{TD}. In the following, the internal dynamics

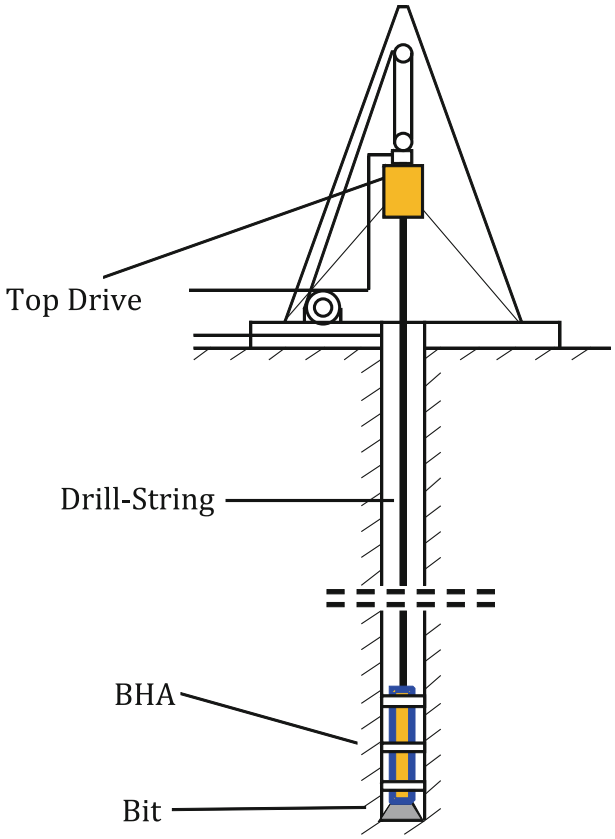

Fig. 1 Schematic setup of drill string

of the top drive will be neglected, and the top drive is modeled as a torque source producing the torque T_{TD}. The desired angular velocity of the top drive is realized via a simple proportional control law by comparing the desired velocity ω_{des} with its current velocity ω_{TD}: $T_{\mathrm{TD}} = K_{\mathrm{P}}(\omega_{\mathrm{des}} - \omega_{\mathrm{TD}})$.

– **Drill String**
The drill string transfers torque from the top drive to the bit and is made up of stell pipes of approx. 10 m length with outside diameters between 0.1 and 0.2 m and wall thickness of 0.03 m, which are screwed together to form the string. It can be modeled as an elastic body of length ℓ, density ρ, and shear modulus G, which is governed by the wave equation.

– **Bottom Hole Assembly (BHA)**
The BHA consists of the drill bit and thick-walled tubulars to apply the necessary pressure on the bit. As the polar second moment of inertia of the BHA is high and thus the torsion is low, the BHA is modeled via a single mass moment of inertia J_{BHA}. The torsion, which is applied on the BHA while drilling due to the nonlinear friction characteristic occuring between bit and rock, is given in (2.1).

2.1 Nonlinear friction

The nonlinear friction between bit and rock and especially the falling friction characteristic is widely believed to be the cause for stick-slip vibrations of drill strings. Different examples for friction characteristics are given, e.g., in [2,3] or [13]. For the simulations in this paper, the friction characteristics are modeled via a piecewise-defined function as implemented in the MATLAB-Simscape Block “Rotational Friction”. The resulting torque $T_{\mathrm{fric}}(\omega_{\mathrm{c}})$ is a function of the angular velocity ω_{c} of the string at the contact point and is defined as

$$T_{\mathrm{fric}}(\omega_{\mathrm{c}}) = \begin{cases} (T_{\mathrm{C}} + (T_{\mathrm{B}} - T_{\mathrm{C}})\mathrm{e}^{(-c_{\mathrm{v}}|\omega_{\mathrm{c}}|)}\mathrm{sign}(\omega_{\mathrm{c}}) + f_{\mathrm{T}}\omega_{\mathrm{c}}, & |\omega_{\mathrm{c}}| \geq \omega_{\mathrm{th}}, \\ (\omega_{\mathrm{c}}/\omega_{\mathrm{th}})\left[f_{\mathrm{T}}\omega_{\mathrm{th}} + (T_{\mathrm{C}} + (T_{\mathrm{B}} - T_{\mathrm{C}})\mathrm{e}^{(-c_{\mathrm{v}}\omega_{\mathrm{th}})})\right], & |\omega_{\mathrm{c}}| < \omega_{\mathrm{th}}. \end{cases} \tag{1}$$

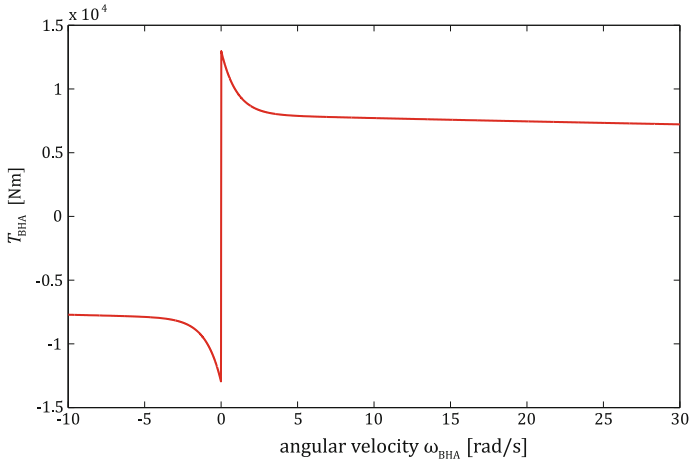

Fig. 2 Nonlinear friction characteristic at BHA

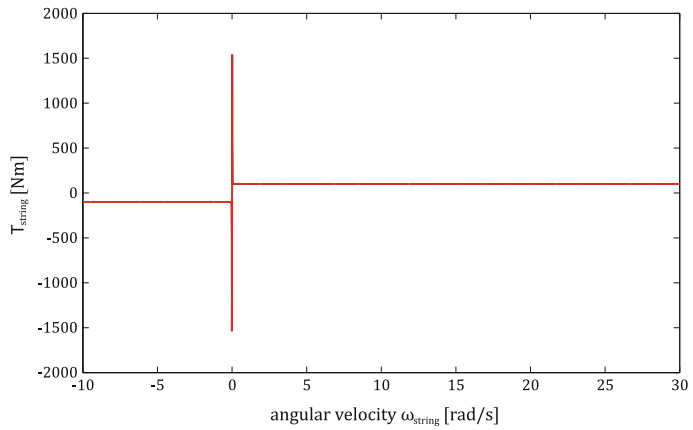

Fig. 3 Nonlinear friction at $x = 3/4 \cdot \ell$

Table 1 Parameters of friction characteristics

$T_{\mathrm{BHA},1}$		$T_{\mathrm{BHA},2}$		T_{string}	
T_{C}:	5,000 Nm	T_{C}:	0.001 Nm	T_{C}:	100 Nm
T_{B}:	10,000 Nm	T_{B}:	3,000 Nm	T_{B}:	4,000 Nm
c_{v}:	1 s/rad	c_{v}:	0.01 s/rad	c_{v}:	100 s/rad
f_{T}:	0.0001 Nms/rad	f_{T}:	0.01 Nms/rad	f_{T}:	0.01 Nms/rad
ω_{th}:	0.01 rad/s	ω_{th}:	0.0001 rad/s	ω_{th}:	0.0001 rad/s

The Coulomb friction is given by T_{C}, and the torque, which is required from breaking the string lose from standstill, is defined by T_{B}. The parameter c_{v} defines how fast the level of the Coulomb friction is reached, and f_{T} defines the viscous friction. The parameter ω_{th} defines the length of the interval in which the discontinuity is approximated via a steep straight line (sticking phase). The friction characteristic $T_{\mathrm{BHA}}(\omega_{\mathrm{BHA}})$ between bit and rock is displayed in Fig. 2. It is realized via a superposition of two curves of (1) in order to approximate measurement data. Another friction contact occuring along the string, $T_{\mathrm{string}}(\omega_{\mathrm{string}})$ is modeled with the friction characteristic displayed in Fig. 3. This curve is characterized by a very low friction value after breaking lose, modeling an effect known as "differential sticking", where the string is pressed strongly to the borehole when the angular velocity is zero due to different pressures in the borehole and the surrounding rock. Parameters are given in Table 1 with $T_{\mathrm{BHA}} = T_{\mathrm{BHA},1} + T_{\mathrm{BHA},2}$.

Table 2 Drill string parameters

Length of drill string ℓ:	2,000 m
Mass moment of inertia of BHA J_{BHA}:	312 kg m^2
Mass moment of inertia of top drive J_{TD}:	25 kg m^2
Proportional gain K_{P}:	100,000 Nms/rad
Internal damping d_i:	0.001 Ns
Polar second moment of area I_{p}:	$1.884 \cdot 10^{-5}$ m^4
Shear modulus of steel G:	$79.6 \cdot 10^9$ N/m^2
Density of steel ρ:	7,850 kg/m^3

2.2 Discretized model

The torsional dynamics of the actual drill string is governed by the wave equation

$$\frac{\partial^2 \phi(x,t)}{\partial t^2} = c^2 \frac{\partial^2 \phi(x,t)}{\partial x^2} \tag{2}$$

with the twist angle ϕ depending on the length coordinate x and time t. The parameter c denotes the propagation speed of a wave in the string and depends on the material due to

$$c = \sqrt{\frac{G}{\rho}}. \tag{3}$$

With the top drive and the BHA being modeled as rigid disks, they occur only in the boundary conditions. The boundary condition for the upper end can be derived from the angular momentum of the top drive and includes the proportional velocity control depending on the desired velocity, and the boundary condition for the lower end can be derived from the angular momentum and includes the friction characteristic. As the friction characteristic is strongly nonlinear, and as additional friction may occur along the string, an analytic solution of the continuous model is not possible except for certain special friction curves (e.g., [16]). Thus, the continuous model has to be discretized. For the numerical simulations, we chose a structure that discretizes the string with a number of lumped mass moments of inertia or rigid disks. This model structure has been widely used in research on drill strings, e.g., in [8,10] or [9]. Some of the parameters listed in Table 2 are taken from [10]. The total number of rigid disks is chosen to 200, with the first rigid disk representing the mass moment of inertia of the top drive J_{TD} and the last rigid disk representing the mass moment of inertia of the BHA J_{BHA}. The string is represented with 198 identical elements with mass moments of inertia $J_2, \ldots, J_{199}$. The elements of the string are coupled via springs and dampers, which correspond to the stiffness and internal damping of the string. External damping of the string is neglected. The equations of motion are summed up in the following with $\dot{\boldsymbol{\phi}} = \boldsymbol{\omega}$:

$$\mathbf{M}\ddot{\boldsymbol{\phi}} + \mathbf{D}\dot{\boldsymbol{\phi}} + \mathbf{K}\boldsymbol{\phi} = \mathbf{g}(\boldsymbol{\omega}). \tag{4}$$

Here, $\mathbf{M}$ is the mass matrix, $\mathbf{D}$ is the damping matrix, and $\mathbf{K}$ the stiffness matrix, $\mathbf{M}$, $\mathbf{D}$ and $\mathbf{K} \in \mathbb{R}^{200\times 200}$:

$$\mathbf{M} = \begin{bmatrix} J_{\mathrm{TD}} & 0 & 0 & \cdots & 0 \\ 0 & J_2 & 0 & \ddots & \vdots \\ 0 & \ddots & \ddots & \ddots & 0 \\ 0 & \ddots & 0 & J_{199} & 0 \\ 0 & \cdots & 0 & 0 & J_{\mathrm{BHA}} \end{bmatrix}, \tag{5}$$

$$\mathbf{D} = \begin{bmatrix} d_1 & -d_1 & 0 & \cdots & 0 \\ -d_1 & (d_1+d_2) & -d_2 & \ddots & \vdots \\ 0 & -d_2 & \ddots & \ddots & 0 \\ \vdots & \ddots & \ddots & (d_{198}+d_{199}) & -d_{199} \\ 0 & \cdots & 0 & -d_{199} & d_{199} \end{bmatrix}, \tag{6}$$

$$\mathbf{K} = \begin{bmatrix} k_1 & -k_1 & 0 & \cdots & 0 \\ -k_1 & (k_1+k_2) & -k_2 & \ddots & \vdots \\ 0 & -k_2 & \ddots & \ddots & 0 \\ \vdots & \ddots & \ddots & (k_{198}+k_{199}) & -k_{199} \\ 0 & \cdots & 0 & -k_{199} & k_{199} \end{bmatrix}. \tag{7}$$

The vector $\mathbf{g}(\boldsymbol{\omega})$ contains all external torques (top drive, nonlinear friction along the string, and nonlinear friction at BHA). Mass moments of inertia J_i, damping coefficients d_j, and spring stiffness k_j are calculated to

$$J_j = \begin{cases} J_{\mathrm{TD}}, & j = 1, \\ \rho I_{\mathrm{p}} \cdot \ell/198, & j = 2, \ldots, 199, \\ J_{\mathrm{BHA}}, & j = 200, \end{cases} \tag{8}$$

$$d_j = \begin{cases} 2dGI_{\mathrm{p}} \cdot 198/\ell, & j = 1, \\ dGI_{\mathrm{p}} \cdot 198/\ell, & j = 2, \ldots, 198, \\ 2dGI_{\mathrm{p}} \cdot 198/\ell, & j = 199, \end{cases} \tag{9}$$

$$k_j = \begin{cases} 2GI_{\mathrm{p}} \cdot 198/\ell, & j = 1, \\ GI_{\mathrm{p}} \cdot 198/\ell, & j = 2, \ldots, 198, \\ 2GI_{\mathrm{p}} \cdot 198/\ell, & j = 199. \end{cases} \tag{10}$$

All parameters are listed in Table 2.

2.3 Resulting dynamics

The resulting dynamics of the model presented in Sect. 2.2 depend strongly on the nonlinear friction characteristic the string is subjected to. In the following, we present two different friction scenarios that result in qualitatively different dynamics of the string. For both scenarios, the equilibrium solution (the whole string turning at a constant velocity) is unstable for the desired angular rotational speed of 15 [rad/s] due to the falling friction slope that acts as a negative damping.

– Scenario one: stick slip at BHA. In this scenario, the friction at the BHA is realized via the nonlinear friction characteristic displayed in Fig. 2. The right-hand side of (4) is thus given by

$$\mathbf{g}(\boldsymbol{\omega}) = (T_{\mathrm{TD}}(\omega_{\mathrm{TD}}), 0, \ldots, 0, -T_{\mathrm{BHA}}(\omega_{\mathrm{BHA}}))^{\mathrm{T}}, \tag{11}$$

with the torque at the top drive T_{TD} and the torque on the BHA $-T_{\mathrm{BHA}}$. The resulting dynamics of the string are depicted in the surface plot Fig. 4. The angular velocity of the string is plotted via the length of the string and the time. While the top drive is rotating with almost constant desired velocity of [15 rad/s], the BHA shows strong stick-slip cycles with overshoot of the angular velocity after a sticking period to more than twice the desired velocity. To clearly mark the stick-slip motion, the evolution of the BHA over time is highlighted with the black line. Additionally, the period and amplitude of the stick-slip cycles are almost constant.

– Scenario two: additonal stick slip at $x = 3/4 \cdot \ell$. In this scenario, an additional friction contact along the string at $x = 3/4 \cdot \ell$ is added to the setup of scenario one, changing the right-hand side of (4) to

$$\mathbf{g}(\boldsymbol{\omega}) = \left(T_{\mathrm{TD}}(\omega_{\mathrm{TD}}), 0, \ldots, -T_{\mathrm{string}}(\omega_{J_{175}}), 0, \ldots, -T_{\mathrm{BHA}}(\omega_{\mathrm{BHA}})\right)^{\mathrm{T}}. \tag{12}$$

The additional friction is implemented according to the nonlinear friction characteristic displayed in Fig. 3. Due to this additional friction, the string now exhibits stick-slip behavior not only at the BHA, but also at the new friction contact. The resulting dynamics are displayed in the surface plot Fig. 5. Due to the new friction contact, the dynamics now show significantly higher complexity than in scenario one and the stick-slip vibrations are much more irregular. Again, the dynamics of the BHA are plotted as a black line.

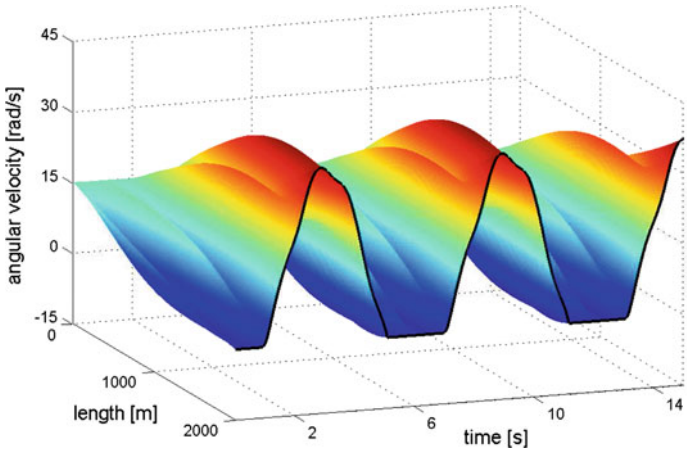

Fig. 4 Drill string dynamics—scenario one

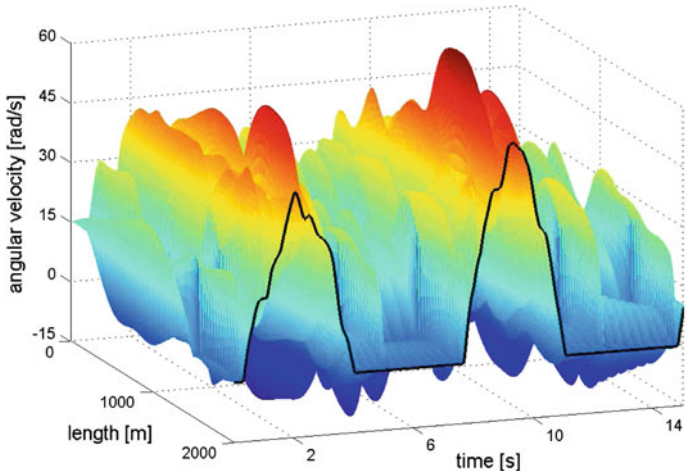

Fig. 5 Drill string dynamics—scenario two

Although only one additional friction contact is added with respect to scenario one, the resulting dynamics vary significantly. As the friction characteristics are not known, a priori and may change during drilling, e.g., due to a change of rock formation, a control law that automatically adapts to the current friction characteristic is desirable. In the following chapter, we derive a control law that is capable of controlling stick-slip vibrations for a wide range of friction characteristics and therefore does not need to be readjusted during drilling. At the same time, no downhole measurements are required for the implementation of the controller.

3 Decomposition of traveling waves in a continuum governed by the wave equation

As mentioned in Chapter 1, the concept for controlling the stick-slip vibrations is based on compensating the wave traveling upwards in the direction of the top drive and thereby extracting energy from the system and preventing reflection at the top drive. Therefore, the evolution of the wave traveling upwards at the location of the top drive has to be calculated. In a series of papers, e.g., in [11] and [12], a concept for the calculation and absorption of traveling waves from measurements is pursued. In this approach, denoted as "wave-based control", an approximation for the calculation of traveling waves using transfer functions is derived on the basis of systems with lumped parameters. In the following, we derive a method for the decomposition of traveling waves, which is based on a one-dimensional continuum governed by the wave equation. With this method, an exact decomposition of the measured dynamics in traveling waves is achieved using delay elements. Thus, the energy flow in the continuum can be decomposed in its two directional components and a maximum energy absorption in the actuator (in case of the drill string the top drive) and a maximum damping of the structure

are ensured. It is worth noting that the control scheme is not based on the complete model of the continuum but uses only the fact that the interval between the two velocity sensors is governed by the wave equation.

We consider a one-dimensional mechanical system of length ℓ, for example the torsional or axial vibration of a rod, with a controlled boundary at $x = 0$ and any arbitrary boundary condition at $x = \ell$. The system is governed by the wave equation:

$$\frac{\partial^2 \phi(x,t)}{\partial t^2} = c^2 \frac{\partial^2 \phi(x,t)}{\partial x^2}. \tag{13}$$

The general solution of the wave equation is

$$\phi(x,t) = f(x - ct) + g(x + ct), \tag{14}$$

with the parameter c being the propagation speed of the wave.

We now look at the short section of the structure $0 < x < x_1$, with $\ell > x_1$. The section $0 < x < x_1$ is considered to be free of disturbances, external forces, or similar. We now assume that at points $x = 0$ and $x = x_1$, velocity measurements $\Omega(x = 0) = \Omega_0$ and $\Omega(x = x_1) = \Omega_1$ are available. In a first step, the measurements are assumed to be free from noise and continuously available. These measurements can be interpreted as time-dependent boundary conditions of the considered section $0 < x < x_1$. Furthermore, the parameter τ is defined such that

$$c\tau = x_1 \tag{15}$$

or

$$\tau = \frac{x_1}{c}. \tag{16}$$

Thus, τ corresponds to the propagation time of the wave between the two measuring points. Inserting the general solution in the time-dependent boundary conditions yields

$$\phi(x = 0, t) = f(-ct) + g(+ct), \tag{17}$$
$$\phi(x = x_1, t) = f(x_1 - ct) + g(x_1 + ct). \tag{18}$$

Defining $\alpha := \frac{\partial}{\partial t} f(x - ct)$ and $\beta := \frac{\partial}{\partial t} g(x + ct)$ results in

$$\Omega_0(t) = \alpha(-ct) + \beta(+ct), \tag{19}$$
$$\Omega_1(t) = \alpha(x_1 - ct) + \beta(x_1 + ct). \tag{20}$$

Because of the known propagation speed, with (15), the following relationships hold:

$$\alpha(x_1 - ct) = \alpha(-c(t - \tau)), \tag{21}$$
$$\beta(ct) = \beta(x_1 + c(t - \tau)), \tag{22}$$
$$\beta(c(t - \tau)) = \beta(x_1 + c(t - 2\tau)). \tag{23}$$

From (19), one obtains using (23)

$$\Omega_0(t - \tau) = \alpha(-c(t - \tau)) + \beta(+c(t - \tau)) \tag{24}$$
$$= \alpha(-c(t - \tau)) + \beta(x_1 + c(t - 2\tau)). \tag{25}$$

This results in

$$\alpha(-c(t - \tau)) = \Omega_0(t - \tau) - \beta(x_1 + c(t - 2\tau)). \tag{26}$$

When now considering the relation for $\Omega_1(t)$, one obtains with (21)

$$\Omega_1(t) = \alpha(x_1 - ct) + \beta(x_1 + ct) \tag{27}$$
$$= \alpha(-c(t - \tau)) + \beta(x_1 + ct). \tag{28}$$

Plucking (26) in (27) results in

$$\Omega_1(t) = \Omega_0(t - \tau) - \beta(x_1 + c(t - 2\tau)) + \beta(x_1 + ct). \tag{29}$$

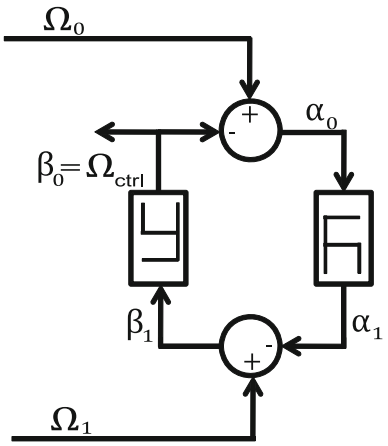

Fig. 6 Dynamical system for decomposition of traveling waves

Hereby, we obtain that $\beta(x_1 + ct)$ can be calculated as a function of the two measurements Ω_0 and Ω_1 and its state lying by 2τ in the past:

$$\beta(x_1 + ct) = \Omega_1(t) - \Omega_0(t - \tau) + \beta(x_1 + c(t - 2\tau)). \tag{30}$$

When the system is, e.g., started from its rest position, $\phi(x, 0) = 0$ and $\Omega(x, 0) = 0$, one obtains the initial conditions

$$\alpha(x = 0, t = 0) = 0, \tag{31}$$
$$\alpha(x = x_1, t = 0) = 0, \tag{32}$$
$$\beta(x = 0, t = 0) = 0, \tag{33}$$
$$\beta(x = x_1, t = 0) = 0. \tag{34}$$

Equivalently, $\alpha(x = 0, t)$, $\alpha(x = x_1, t)$, $\beta(x = 0, t)$, $\beta(x = x_1, t)$ can be determined continuously using the measurements Ω_0 and Ω_1.

The resulting dynamical system is displayed in Fig. 6 and shows some special characteristics because of the fact that the transfer elements are pure time delays.

When looking at the systems dynamics in the Laplace domain, by defining the Laplace variable s and the transfer function G_τ for a time delay τ to

$$G_\tau = \mathrm{e}^{-\tau s} = \lim_{n\to\infty} \frac{1}{(1 - \frac{-\tau s}{n})^n}, \tag{35}$$

the transfer function from the input signals $\Omega_0(s)$ and $\Omega_1(s)$ to the state $\beta(x = 0, s)$ can now be determined using

$$\alpha(x = 0, s) = \Omega_0(s) - \beta(x = 0, s), \tag{36}$$
$$\alpha(x = x_1, s) = G_\tau \alpha(x = 0, s), \tag{37}$$
$$\beta(x = x_1, s) = \Omega_1(s) - \alpha(x = x_1, s), \tag{38}$$
$$\beta(x = 0, s) = G_\tau \beta(x = x_1, s) \tag{39}$$

and

$$\begin{aligned}\beta(x = x_1, s) &= \Omega_1(s) - \alpha(x = x_1, s) = \Omega_1(s) - G_\tau \alpha(x = 0, s) \\ &= \Omega_1(s) - G_\tau(\Omega_0(s) - \beta(x = 0, s)),\end{aligned} \tag{40}$$
$$\beta(x = 0, s) = G_\tau \beta(x = x_1, s) = G_\tau[\Omega_1(s) - G_\tau(\Omega_0(s) - \beta(x = 0, s))] \tag{41}$$

to

$$\beta(x=0,s) = \frac{G_\tau \Omega_1(s) - G_\tau^2 \Omega_0(s)}{(1-G_\tau^2)}. \tag{42}$$

It is worth noting that, as the inversion of the time delay

$$(\mathrm{e}^{-\tau s})^{-1} = \mathrm{e}^{\tau s} \tag{43}$$

leads to a noncausal transfer function, the dynamical system is causal only in forward time and thus the solution is unique only in forward time, i.e., current system states allow to calculate the current inputs, but not the evolution of the inputs in backward time.

3.1 Impact of an initial deformation

An initial deformation between the two measurement points at time $t_0 = 0$ leads to a static deviation in the dynamics of the system for the decomposition of traveling waves (Fig. 6). Essentially, this results in a constant positive offset on one side of the dynamical system and a constant negative offset on the other side. We noticed this effect in our experimental setup of a drill string, as, due to friction in the sensor bearings, there is always an initial deformation between the two sensors.

The influence of the initial deformation on the constant offset can be shown with the following calculations: an exponentially decaying initial deformation of the form e^{-t} of the sensor signal $\Omega_1(t)$ is considered. For $\Omega_0 = 0 = \text{const}$, Ω_1 is represented in the Laplace domain as

$$\Omega_1(s) = \frac{1}{s+1}. \tag{44}$$

Plucking (44) in (42) and using

$$\lim_{t\to\infty} f(t) = \lim_{s\to 0} sF(s) \tag{45}$$

results in

$$\lim_{t\to\infty} \beta(x=0,t) = \lim_{s\to 0} s \frac{G_\tau}{(1-G_\tau^2)} \frac{1}{(s+1)} = \frac{1}{2\tau}. \tag{46}$$

The result shows that the constant offset caused by an initial deformation depends strongly on τ. Especially, the constant offset gets large for small values of τ. As an example, for $\tau = 0.001$, the constant offset results in $\beta(x=0,t)(t\to\infty) = 500$.

A remedy for this situation is the application of a simple high-pass filter, either within the loop or for the resulting control signal. Alternatively, the static offset caused by an initial deformation can be subtracted in the dynamical system. This is only possible if, next to τ, the initial deformation is known.

3.2 Measurement error

For additive or multiplicative errors of the sensors, the dynamics of the wave decomposition will diverge linearly. For the case $\Omega_0 = 0$, $\Omega_1(t) = c_m$, or $\Omega_1(s) = \frac{c_m}{s}$ in the Laplace domain with $c_m \neq 0$, one obtains with (42)

$$\beta(x=0,s) = \frac{G_\tau}{1-G_\tau^2} \frac{c_m}{s}. \tag{47}$$

As the limit value does not exist in this case, (45) cannot be applied. However, one obtains a transfer function of the form

$$\beta(x=0,s) = \frac{(\text{h.o.t}) + 2\tau s + 1}{(\text{h.o.t.}) + 2\tau s} \cdot \frac{c_m}{s}, \tag{48}$$

so the long-term dynamical behavior is determined by

$$\beta(x=0,s) \approx \frac{c_m}{2\tau s^2}, \tag{49}$$

which corresponds to a linear divergence in the time domain. A multiplicative sensor error therefore does not lead to exponential instability, but to a linear divergence with gradient $\frac{c_m}{2\tau}$.

3.3 Frequency range of decomposed waves

Finally, it is worth mentioning that the frequency range in which the traveling waves can be decomposed does not depend on the distance between the sensors or the resulting time interval τ. Especially, waves with wave lengths $\lambda >> \tau c$ can be identified. The upper bound of the frequency range is determined by the sensor sampling rate (or the corner frequency of a low-pass filter used to filter discretization noise). For sampling rates $\tau_s << \tau$, waves with wavelengths $\lambda < \tau c$ can be decomposed.

4 Results from numerical simulations

The controller for the stabilization of the stick-slip vibrations is implemented following Chapter 3. As inputs for the controller, the velocity of the top drive Ω_0 and the velocity of the first element of the string (corresponding to a distance of 5 m below the top drive) Ω_1 are measured. Thus, no downhole measurements are required and external knowledge of the model, especially of the forces acting on the string neither have to be measured nor known for the stabilization control. This is a major advantage compared with known control concepts in drill string dynamics. The delay parameter τ is set to 0.0015 s, which is calculated using the propagation speed of a torsional wave in steel

$$c_{\text{steel}} = \sqrt{\frac{G_{\text{steel}}}{\rho_{\text{steel}}}} = \sqrt{\frac{79.6 \cdot 10^9\,(\text{N/m}^2)}{7,850\,(\text{kg/m}^3)}} \approx 3{,}184\,(\text{m/s}) \tag{50}$$

and corresponds to the traveling time of the wave in the string for a length of approx. 5 m. In order to stabilize the undesired vibrations, the decomposed velocity β_0 is now added to the constant desired velocity of the top drive. The signal from the stabilization controller is filtered with a second-order butterworth high-pass filter with corner frequency of 0.02 Hz to allow for the constant velocity and slow variations of the desired velocity to pass the controller; otherwise, the controller would stabilize the velocity at speed zero. A low-pass butterworth filter of order six and corner frequency of 80 Hz is used to filter high-frequency noise from discretization. The location of the filters is displayed in Fig. 7 (LPF: Low-pass filter, HPF: High-pass filter). Thus, undesired vibrations in the range between 0.02 and 80 Hz can be stabilized. The resulting stabilization controller then compensates the wave traveling in direction of the top drive, preventing reflection back into the system, as $\alpha(x = 0, t)$ will be zero for $\Omega_0 = \beta_0$. The complete control setup is displayed in Fig. 7.

4.1 Scenario one

For the scenario of simple stick slip at the BHA, the results of the application of the control concept are displayed in Fig. 8. The plot is a continuation of Fig. 4 and thus starts at $t = 5$ s. Again, the evolution of the BHA is plotted as a black line. The plane, which is spanned by the dashed lines, marks the time when the controller is turned on. From that point, the desired velocity at the top drive is no longer constant, but the addition of the constant velocity and the wave traveling in the direction of the top drive. It is clearly visible from Fig. 8 that the stick-slip vibrations are instantly cured as almost all vibration energy is absorbed within the time of one stick-slip period. With the controller being turned on, after a short while, the whole string turns at the constant desired velocity of 15 [rad/s]. As from Fig. 8, the evolution of the velocity of the top drive is not very well visible, Fig. 9 shows the evolution of the top drive (bright line) and the evolution of the BHA (black line).

4.2 Scenario two

For the second scenario, the dynamics of the string are significantly more complex, as stick slip occurs not only at the BHA, but also along the string. However, the control concept can handle the more complex case as well. Results for this case are displayed in Fig. 10. Again, this plot is a continuation of Fig. 5 and thus starts at $t = 5$ s. The evolution of the BHA is plotted as a black line, and the plane spanned by the dashed lines marks the point of time when the controller is turned on. Although the dynamics are more complex in this case, the whole string is stabilized and turns at the constant desired angular velocity after only about one period of the stick-slip vibration after the controller has been turned on. Figure 11 shows the corresponding evolution of the top drive (bright line), the BHA (black line), and the location along the string at $x = 3/4 \cdot \ell$

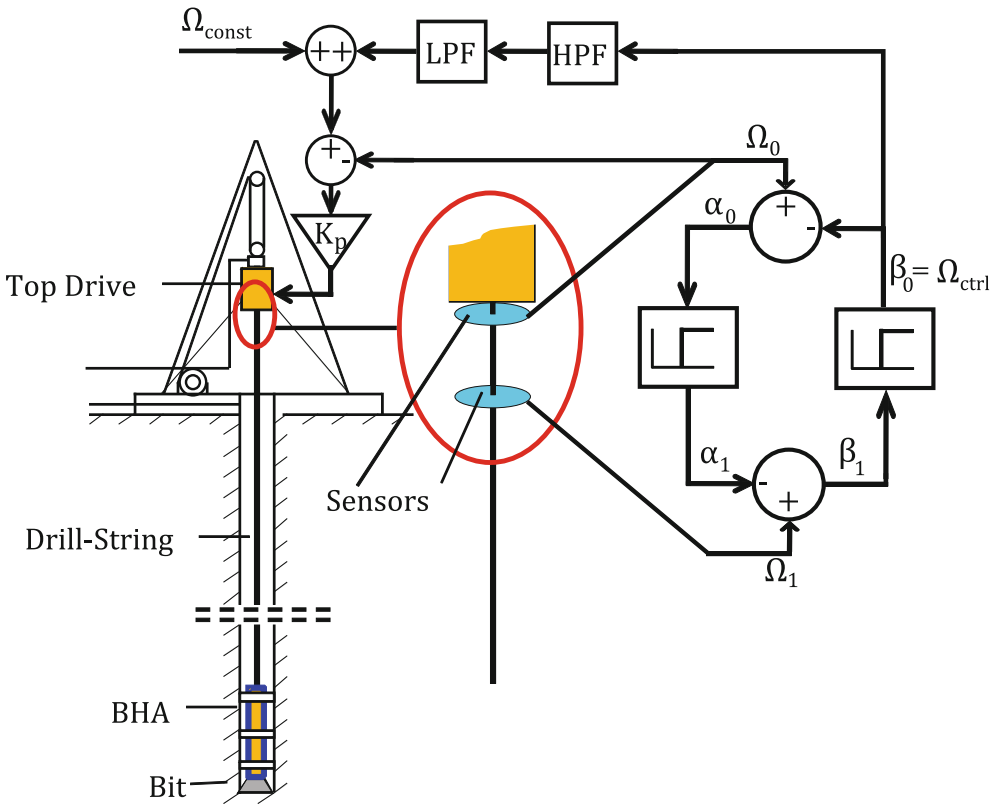

Fig. 7 Drill string, position of sensors and controller

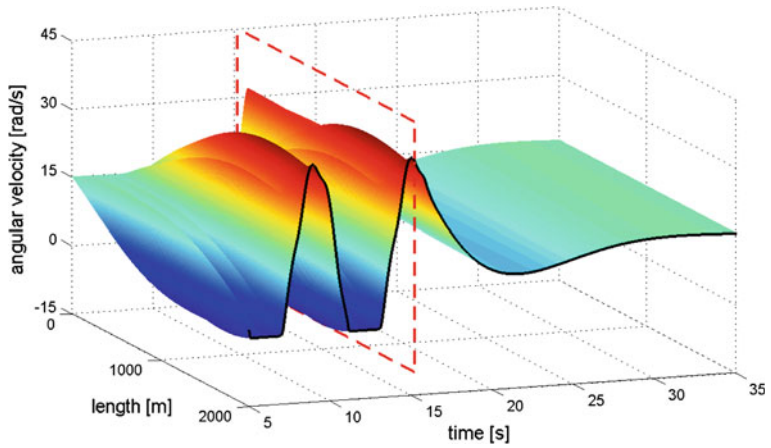

Fig. 8 Drill string vibrations—scenario one controlled

where the second stick-slip contact occurs. The trajectory of the top drive is now significantly more complex, resembling the fact that the wave traveling in the direction of the top drive now consists of a much richer frequency spectrum. This second example shows another benefit of the control scheme next to the fact that no downhole measurements are required; it adapts to the current external loads of the system without having to be retuned, as the control scheme is not based on the drill string model and knowledge about the external forces acting on the string is not required. In this context, it is worth mentioning that the location of the contact point of the second friction contact at $x = 3/4 \cdot \ell$ is chosen arbitrarily and that stabilization of the string is not sensitive to the location of the contact point. In simulation scenarios with other contact points, e.g., $x = 1/2 \cdot \ell$, the capability of the controller to stabilize the string was not affected.

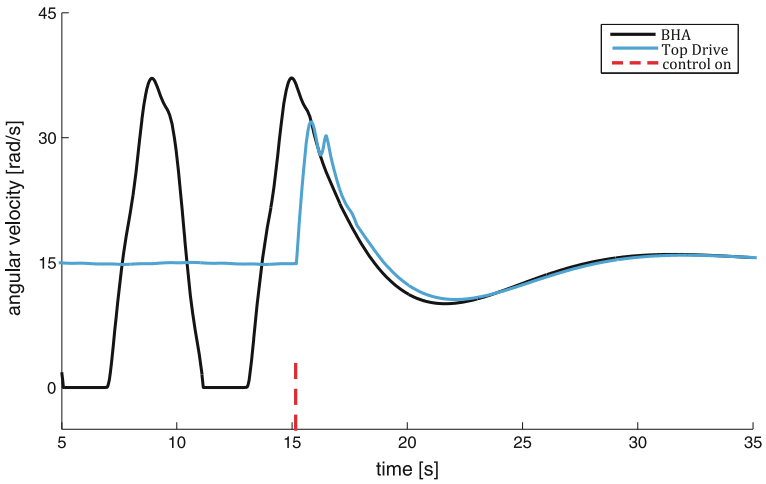

Fig. 9 Angular velocity of top drive and BHA—scenario one controlled

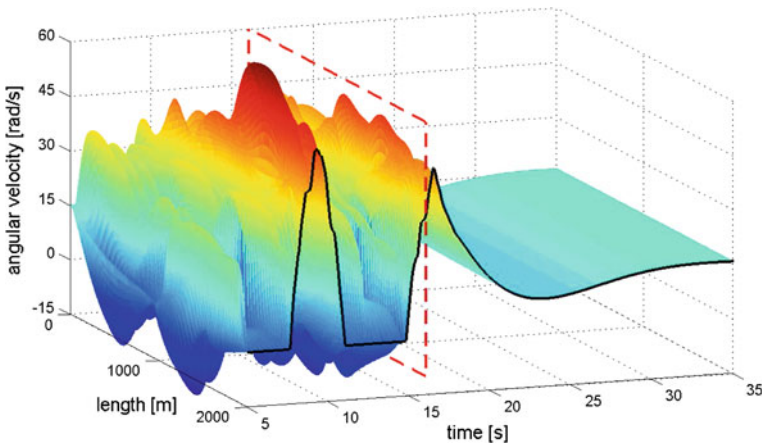

Fig. 10 Drill string vibrations—scenario two controlled

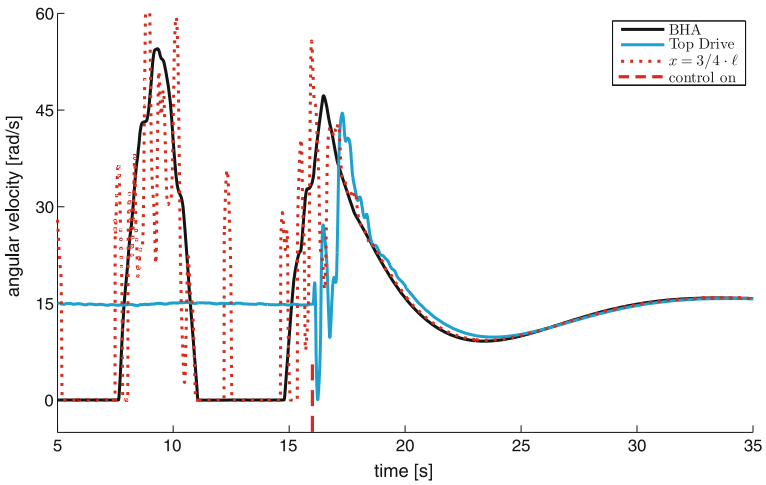

Fig. 11 Angular velocity of top drive and BHA—scenario two controlled

5 Results from experimental setup

The goal of the experimental setup of a small-scale model of the drill string is to demonstrate that the control concept derived in Chapter 3 is not only applicable for numerical models, but can be realized with currently available technology. As the control concept requires fast and accurate measurements, the focus is on the realization of the control loop and the feedback of the control signal to the actuator. The drill string model at the Institute of Mechanics and Ocean Engineering consists of a brass string with total length of 10 m and diameter of 0.005 m, thus obtaining the torsional stiffness of a real-sized drill string. The high mass moment of inertia of the BHA is modeled with a brass disc as shown in Fig. 12. The top drive is realized via an AC Motor, the friction between the bit and rock is modeled via a scaled version of friction curve of Fig. 2 and is applied via an AC Motor. Angular velocities of the drill string are measured with angular encoders at the top, the bottom, and at three equidistant points along the string. The control concept is realized in Labview on a standard PC that runs a real-time operating system (LabView RT), with the communication between sensors and RT system via an FPGA and communication via RT system and AC Motors via PROFIBUS. A schematic setup of the string and the connected hardware and software is shown in Fig. 13.

The speed of torsional waves in brass is given by

$$c_{\text{brass}} = \sqrt{\frac{G_{\text{brass}}}{\rho_{\text{brass}}}} = \sqrt{\frac{27.5 \cdot 10^9\ (\text{N/m}^2)}{8{,}363\ (\text{kg/m}^3)}} \approx 1{,}813\ (\text{m/s}). \tag{51}$$

The control algorithm based on the wave decomposition is implemented using the two upper angular encoders. The first encoder is placed directly underneath the actuator. The position of the second encoder is chosen such that the traveling time of a torsional wave between the two encoders is one ms; therefore, it is placed at approximately 1.8 m below the first encoder. Due to the choice of the nonlinear friction characteristic, the string shows strong stick-slip vibrations when the top drive is controlled to operate at a constant velocity via a proportional control law, which is implemented on the SIMOTION Controller. The experimental setup is thus configured to resemble the first scenario described in Chapter 2.3. Here, we use a high-pass butterworth filter of order four and corner frequency of 0.2 Hz to allow the constant velocity to pass the vibration filter and to allow changes in the angular velocity set by the driller. A low-pass butterworth filter of order six and corner frequency of 300 Hz is used to filter high-frequency noise (e.g., from discretization of measurements).

Figure 14 shows that the experimental setup exhibits stick-slip vibrations when uncontrolled; however, when the stabilization controller is turned on (indicated by the dashed vertical line), the stick-slip vibrations decay rapidly and the string turns at an almost constant velocity. The bright line indicates the velocity of the top drive, and the black line indicates the velocity of the BHA.

Figure 15 shows that the stick-slip vibrations set on again when the stabilization controller is turned off, showing that rotation at the desired angular velocity of 15 rad/s is unstable when uncontrolled. Here, the dashed vertical line marks the time when the controller is turned off, while the bright line indicates the velocity of the top drive and the black line the velocity of the BHA.

The results from the experimental setup thus demonstrate that the accuracy and speed of currently available sensors are adequate to realize the control concept derived in Sect. 3.

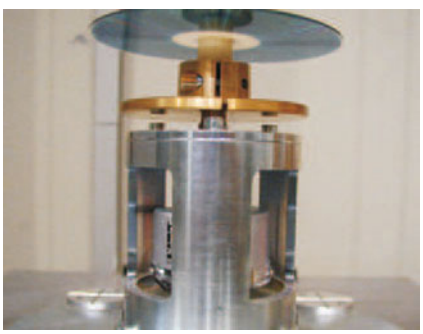

Fig. 12 Detail of experimental setup: BHA and angular encoder

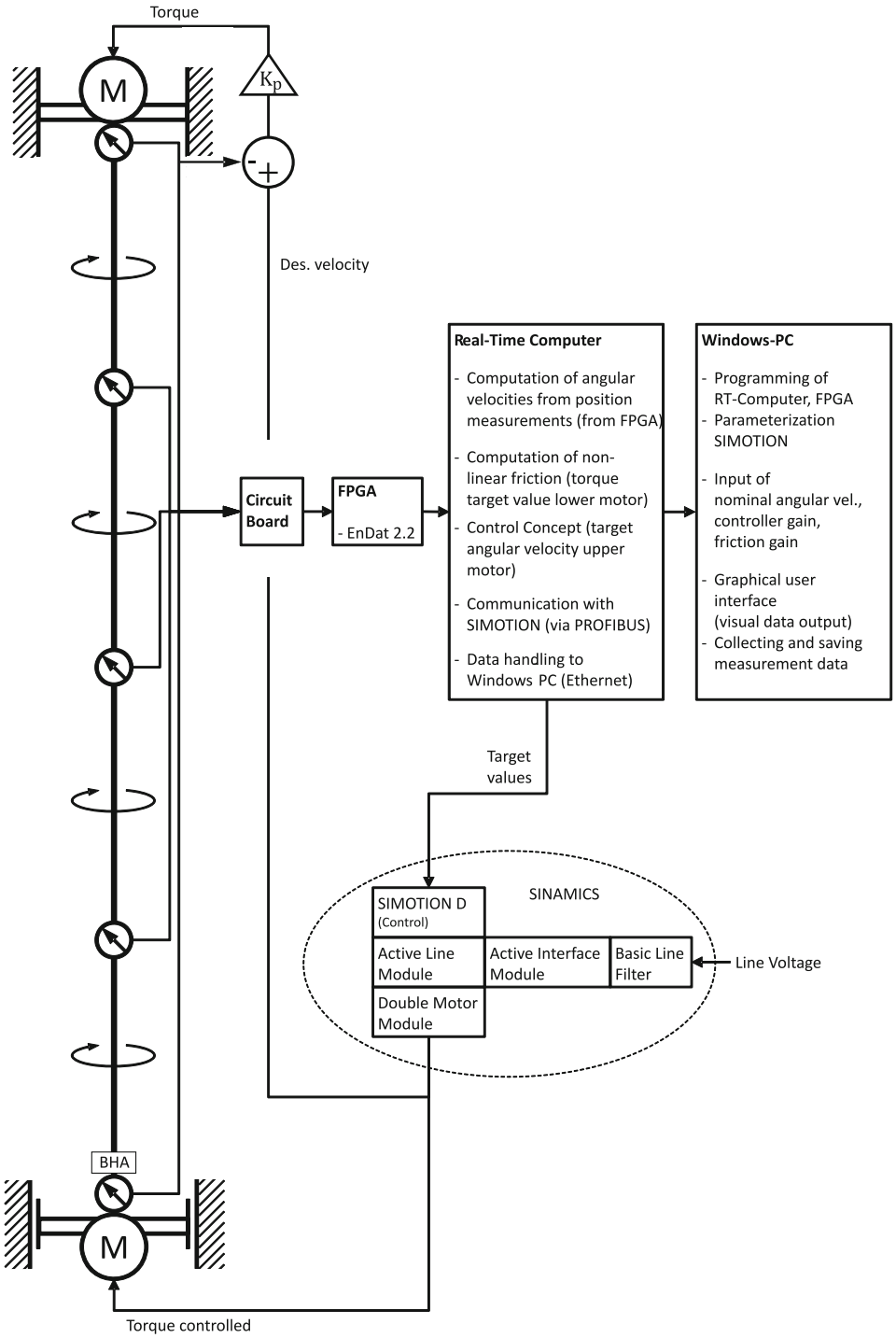

Fig. 13 Schematic description of experimental setup

6 Conclusion

We showed a new approach for stabilization and vibration mitigation for torsional vibrations in drill strings. The control law was derived, based on a continuum governed by the wave equation, by decomposing the dynamics into a wave traveling in the direction of the actuator and a wave traveling away from the actuator. In order to realize the decomposition into two traveling waves, only two sensors are required. Further, the

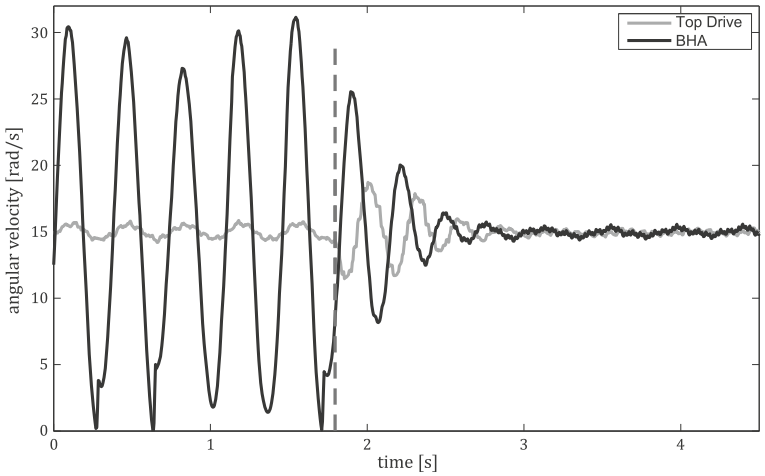

Fig. 14 Measured angular velocities at experimental setup—control turned on

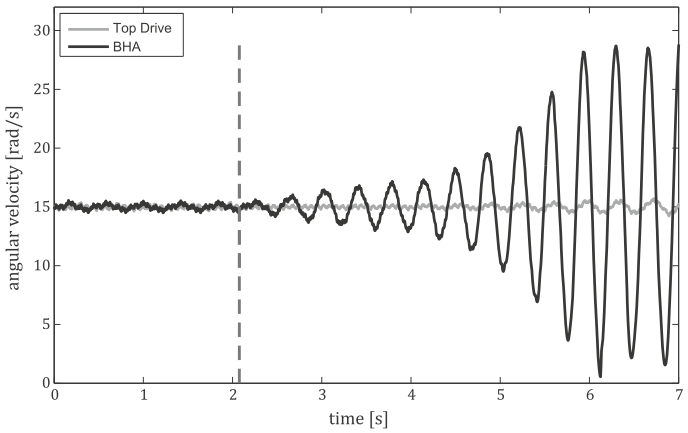

Fig. 15 Measured angular velocities at experimental setup—control turned off

sensors can be mounted very close to the actuator, while the controller stabilizes the whole string, so downhole measurements are not necessary.

The wave traveling in the direction of the actuator can hence be absorbed by the actuator, thereby extracting energy from the system and removing reflection at the top drive. The reflection coefficient at the top drive can be realized to zero over the frequency range of the relevant frequencies; therefore, the control algorithm is capable of covering a wide range of unknown external excitations without the need of re-calibrating the controller. At the same time, it is not relevant whether only one mode or multiple modes are excited or where along the string the external forces are applied. The vibrations can be caused by local or distributed forces, as long as the forces causing the vibrations are not within the range between the two sensors. Performance of the proposed control algorithm was shown for a numerical drill string model. By implementing the control law in a small-scale experimental setup of a drill string with a length of 10 m, we demonstrated that realization of the proposed control concept is possible with currently available technology. The theoretical approach is not restricted to the use in drill strings, but could be used for any system governed by the wave equation.

References

1. Aldred, W., Plumb, D., Bradford, I., Cook, J., Gholkar, V., Cousins, L., Minton, R., Fuller, J., Goraya, S., Tucker, D.: Managing drilling risk. Oilfield Rev. **11**(2), 2–19 (1999)
2. Balanov, A., Janson, N., McClintock, P., Tucker, C., Wang, R.W.: Bifurcation analysis of a neutral delay differential equation modelling the torsional motion of a driven drill-string. Chaos Solitons Fractals **15**, 381–394 (2003)
3. Brett, J.F.: The genisis of torsional drillstring vibrations. SPE Drill. Eng. **7**, 168–171 (1992)

4. Dawson, R., Lin, Y., Spanos, P.: Drill-string stick-slip oscillations. In: Proceedings of the 1987 Conference of the Society of Experimental Mechanics (1987)
5. Halsey, G., Kyllingstad, A., Kylling, A.: Torque feedback used to cure slip-stick motion. In: SPE Annual Technical Conference and Exhibition, Houston, Texas, 2–5 October (1988)
6. Jansen, J., Van den Steen, L.: Active damping of self-excited torsional vibrations in oil well drillstrings. J. Sound Vib. **179**, 647–668 (1995)
7. Karkoub, M., Zribi, M., Elchaar, L., Lamont, L.: Robust μ-synthesis controllers for suppressing stick-slip induced vibrations in oil well drill strings. Multibody Syst. Dyn. **23**, 191–207 (2010)
8. Kreuzer, E., Kust, O.: Analysis of long torsional strings by proper orthogonal decomposition. Arch. Appl. Mech. **67**(1), 68–80 (1996). doi:10.1007/BF00787141
9. Kreuzer, E., Steidl, M.: Model order reduction of a drill-string-model with self-excited stick-slip vibrations. In: Kalinski, P.K.J. (ed.) PAMM Special Issue: 80th Annual Meeting of the International Association of Applied Mathematics and Mechanics (GAMM), Gdansk 2009, vol. 9, pp. 295–296. doi:10.1002/pamm.200910121 (2009)
10. Kust, O.: Selbsterregte Drehschwingungen in schlanken Torsionssträngen. PhD thesis, Technische Universität Hamburg–Harburg (1998)
11. O'Connor, W.: Wave-based analysis and control of lump-modeled flexible robots. IEEE Trans. Robotics **23**(2), 342–352 (2007)
12. O'Connor, W.J., McKeown, D.J.: Time-optimal control of flexible robots made robust through wave-based feedback. J. Dyn. Syst. Meas.Control **133**(1). doi:10.1115/1.4002714 (2011)
13. Pavone, D.: Method and system for controlling the rotary speed stability of a drill bit. US Patent 5507353 (1996)
14. Serrarens, A., van de Molengraft, M., Kok, J., van den Steen, L.: H_∞-control for suppresing stick-slip in oil-well drillstrings. IEEE Control Syst. Mag. **18**, 19–30 (1998). doi:10.1109/37.664652
15. van den Steen, L.: Suppressing stick-slip-induced drill-string oscillations: a hyper stability approach. PhD thesis, University of Twente, Netherlands (1997)
16. Stingl, B.: Analytische Untersuchung von laufenden Wellen bei Stick-Slip-Schwingungen in Torsionsstäben. Diplomarbeit, Institut für Mechanik und Meerestechnik, Technische Universität Hamburg–Harburg (2009)
17. Struck, H.: Modellierung, Simulation und aktive Dämpfung selbsterregter Schwingungen eines gekrümmten Torsionsstranges. PhD thesis, Technische Universität Hamburg–Harburg (2004)
18. Tucker, R., Wang, C.: On the effective control of torsional vibrations in drilling systems. J. Sound Vib. **224**, 101–122 (1999)